CHAPTER 3

THEORY

Steel Making Process.

The blast furnace is the primary unit for reducing iron ore to elemental iron. The charge, which is a mixture of iron ore, limestone and coke, is blasted with preheated air in the correct amount to generate heat and form carbon monoxide needed to reduce the ore to molten iron and slag. The final composition of the iron depends a great deal on the type of ore used, but control of the final composition is possible in the blast furnace itself, except for manganese and phosphorus which cannot be greatly varied. Table 3.1 shows the steel making process.

Table 3.1 The Process of Steel Making

Blast furnace ↓	* Producing hot metal: $Fe_2O_3 + 3CO \rightarrow 2Fe + 3CO_2$ and $Fe_2O_3 + 3C \rightarrow 3CO + 2Fe$ Fe at this stage is called hot metal and it includes many impurities such as P, S, Si and its carbon content is high.
↓ Torpedo car	* This container is called torpedo car and is used for hot metal treatment. (1) desiliconization by adding FeO, Fe_2O_3 (2) desulphurization by adding FeO, Fe_2O_3, O_2 (3) dephosphorization by adding CaO, CaFe Na_2CO_3
↓ Converter	* Carbon is removed in this container by blowing O_2 gas. CaO is also added into the converter to get rid of oxides such as SiO_2, Al_2O_3 which are impurities.

↓

Ladle

* MnFe, SiF, Al is added to the ladle to get rid of residual O_2 gas. Ni, Cr, W, Mo, V, Co, Ti, Nb and so on are also added in order to improve the steel quality. When the molten steel moves to the ladle from the converter, the molten steel exhibits temperature distribution which lowers steel quality. So the porous plug is used to maintain uniform temperature by stirring with Ar gas, in order to unify the composition of molten steel.

↓

Tundish

* The purpose of this container is to maintain a suitable velocity of molten steel to mould uniformly. If the casting speed of molten steel changes, good uniform steel cannot be obtained.

↓

Mould

* Liquid steel, after having been refined in an oxygen vessel (top-blown or bottom-blown) or in an arc furnace, must be cast to render a solid. The traditional method of casting into cast-iron ingots of dimensions 500 x 300 x 3,000 mm (or there about) are being replaced by casting into a copper mould, cooled by water. After solidification in the mould, the steel is drawn down by rollers and then cut off by oxygen torches after the desired length of material has been cast. Care has to be taken to support the solidifying metal, as it is not completely solid across the whole cross section until several meters have been drawn through the mould.
A wide range of shapes may be cast continuously. Billets, blooms and slabs may be cast and even, in specialized machines, "dog-bone" cross sections. The range of sizes (in cross-section) normally associated with

these shapes are given in table 3.2.

Table 3.2 A Wide Range of Shapes of Cast Steel

Name	Range of cross section (mm)
Billet	100 x 100 to 150 x 150
Bloom	300 x 300 to 500 x 500
Slab	200 x 1,500 to 300 x2,500

Application of Porous Ceramic Refractory.

Molten steel coming out of the converter includes many impurities, such as C, H_2, O_2, S, P and non-metal inclusions which come from refractories. In order to get clean steel, these impurities must be removed, and the porous plug is used for this purpose. The mechanism of removing the impurities is to stir with Ar gas that is injected through the porous plug and to float the impurities. Other purposes of using the porous plug are to unify the temperature of molten steel and to unify the components which are added into the molten steel in order to get high quality steel, such as CaH_2 , CaO, Al, Si and so on.

To meet the growing demand for high-quality steel products, conventional ladle linings with Roseki firebricks were replaced by linings with high-silicon, zircon and high-alumina bricks, which have in turn been replaced by linings with basic bricks.

On the other hand, mechanized lining methods and partial repair without replacing work base using monolithic refractories have found wide application to save manpower and to reduce consumption of refractories per unit product.

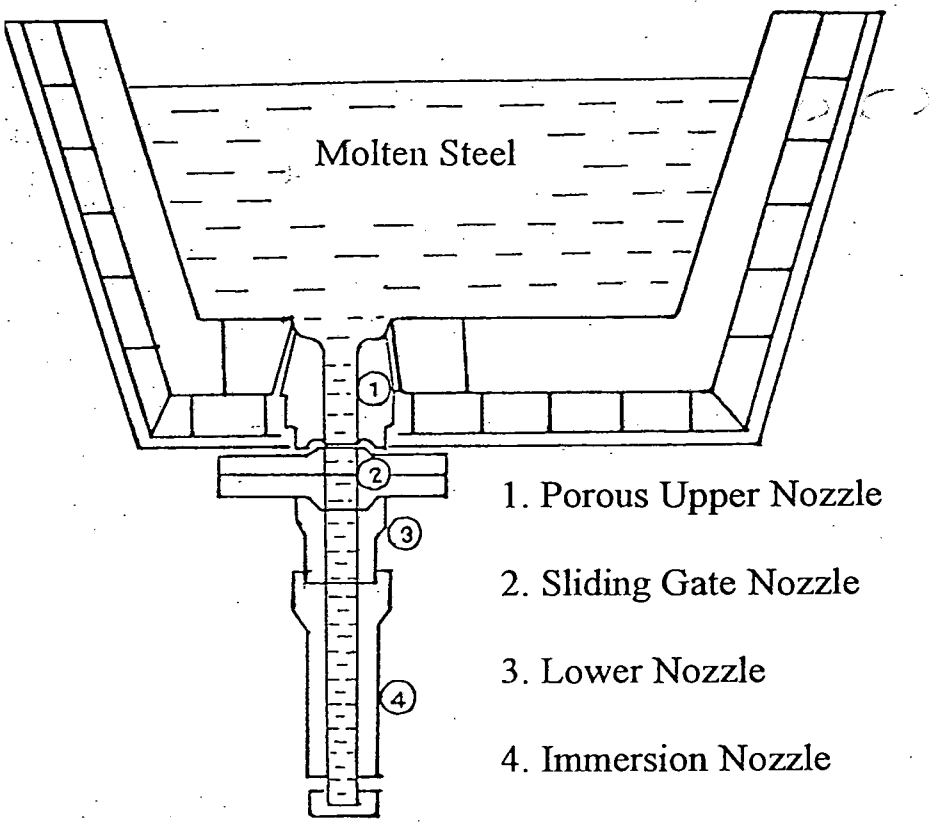

Figure 3.1 Cross Section of the Refractory Part of Tundish

Another application of porous refractories is the porous upper nozzle of the tundish. The purpose of the porous nozzle is to prevent nozzle from clogging due to sticking of non-metallic inclusions onto the inner surface of the nozzle.

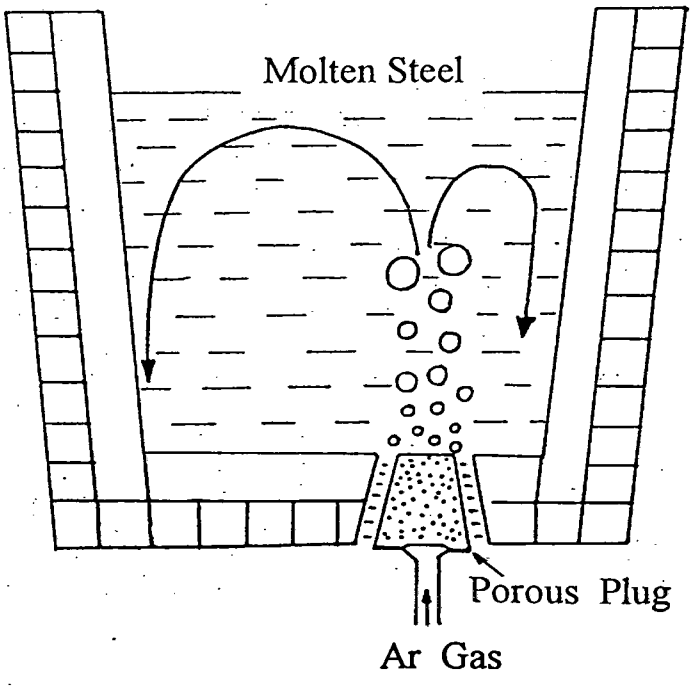

Figure 3.2 Ladle Assembly with Porous Plug

Since the tundish is the vessel used in the final stage of steel-making, it has a direct effect on the quality and yields of steel. Accordingly, tundish refractories must be produced by up-to-date technology under close quality control. Meanwhile, monolithic lining methods have found wide application to save manpower in tundish lining and to improve the lining efficiency.

Though the sliding nozzle was originally developed as a stopper for ladle, it has found gradual application in the tundish for control of metal flow. Sliding nozzle refractories must be high in spalling resistance, wear resistance and erosion resistance, to withstand frequent sliding operations and to meet multiple continuous castings. Moreover, these refractories must withstand the gas that is blown from the sliding nozzle plate and the top nozzle at the time of immersion nozzle replacement as well as to prevent the clogging of the immersion nozzle with alumina.

Kozeny-Carman Theory.

A sintered porous medium is composed of many discrete particles with different shapes and sizes, as shown in figure 3.3. The packing density of the medium is high and its structure is complicated. The porous medium can for practical purposes be simplified as an assembly of many parallel tiny channels or of many uniformly spaced spherical particles of equal sizes. The flow resistance can then be predicted by analogy with that of the straight circular tube or with that of flow around submerged spheres.

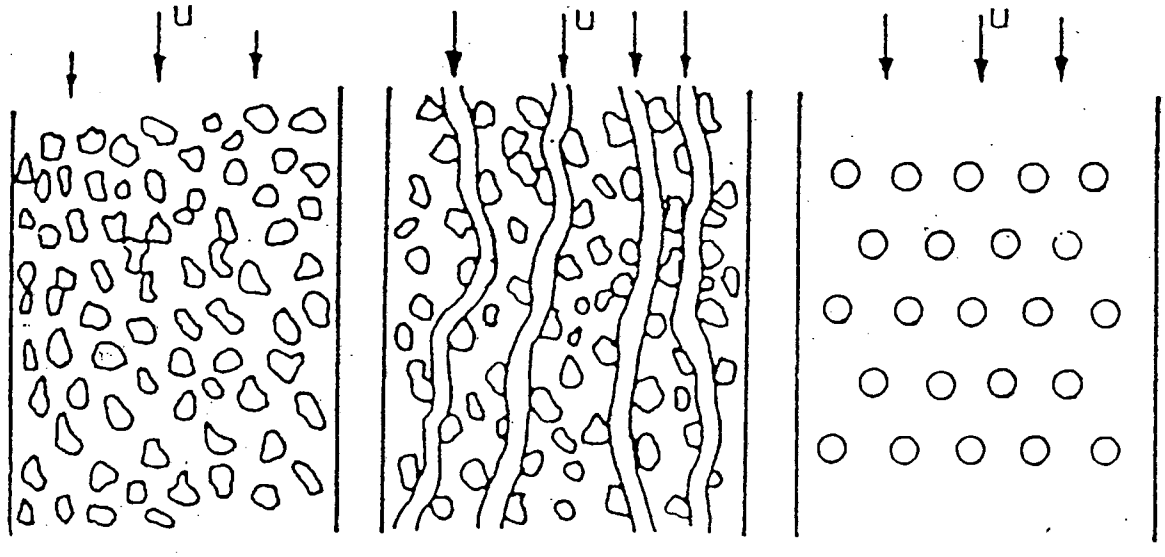

Figure 3.3 Models of Porous Medium

If the porous system is assumed here to be a bundle of parallel identical tiny channels with non-circular cross sections, the pressure drop of the system is equal to that of one of these channels.

A porous refractory is a sintered body made up of an aggregate of particles with different sizes and shapes. Thus the actual flow pattern is very different from that of a simple structure, such as a cylindrical tube. Nevertheless, pressure drop of the medium can be predicted by either a channel model or a drag theory. The former assumes the flow area of the medium as a bundle of channels and pressure drop is related to the specific surface area and porosity of the medium.

It was realized by Dupuit (1963) that the apparent linear flow velocity u must be less than the actual velocity u_e in the pore space. If the pore space is isotropically and randomly distributed, the porosity of any layer of infinitesimal thickness normal to the direction of flow will be equal to ε , the porosity of the body as a whole. Since for such a layer, the fractional pore volume is equal to the fractional pore area, we have:

$$u_e = u/\varepsilon \qquad (3.1)$$

For non-circular channels Schiller (1923) introduced a hydraulic radius m, defined as follows:

$$m = \frac{\text{cross-sectional area normal to flow}}{\text{wetted periphery}} \qquad (3.2)$$

For a channel of uniform cross-section, we can write also:

$$m = \frac{\text{cross-sectional area x tube length}}{\text{wetted periphery x tube length}} \qquad (3.3)$$

$$m = \frac{\text{volume filled with fluid}}{\text{wetted surface}} \qquad (3.4)$$

$$m = \frac{\text{total pore volume}}{\text{total surface area of particles in porous medium}} \qquad (3.5)$$

$$m = \frac{\text{porosity}}{\text{specific surface area based on the volume of porous medium}} \qquad (3.6)$$

$$m = \varepsilon / S_B = \varepsilon / S_V(1 - \varepsilon) \qquad (3.7)$$

Here S_B and S_V are the specific surface areas based on packed bed volume and particle volume, respectively.

The value of m calculated from equation (3.7) equals one-quarter of the tube diameter for circular tubes and approximately one-quarter of the equivalent diameter for other cross-sectional shapes.

$$m = \frac{(\pi/4)d^2L}{\pi dL} = d/4 \qquad (3.8)$$

According to Carman's tortuosity model, the time required for fluid to pass through an equivalent channel is equal to the actual penetration time to pass straight through the bed. Hence, the following relation is obtained:

$$L_e / u_e = L / (u/\varepsilon) \qquad (3.9)$$

$$u_e = (L_e / L)(u / \varepsilon) \qquad (3.10)$$

L_e / L is the ratio of the equivalent channel length to the bed thickness and it is called tortuosity as illustrated in figure 3.4.

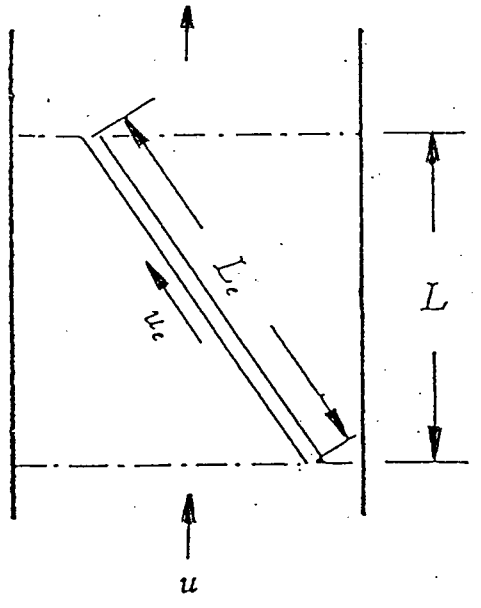

Figure 3.4 Relation between Equivalent Channel Length and Bed Thickness

When fluid with density ρ and viscosity μ flows laminarly through a straight tube with diameter d, Fanning ' s friction factor f and length L, the pressure drop ΔP is expressible by the so-called Hagen-Poiseuille equation for laminar flow and Fanning's equation:

Hagen-Poiseuille equation : $$\Delta P = \frac{32L\mu u}{d^2} \qquad (3.11)$$

Fanning's equation : $$\Delta P = \frac{4fL}{d} \cdot \frac{\rho u^2}{2} \qquad (3.12)$$

Assuming that the pores of permeable refractories are uniform and cylindrical, we can apply Hagen-Poiseuille equation to

estimate pressure drop in laminar flow. Flow rate Q (volume per unit time) through a pipe of diameter d is given by:

$$Q = \frac{\pi (d/2)^4}{8\mu} \cdot \frac{\Delta P}{L_e} \tag{3.13}$$

Average velocity u_e, is calculated from the following equation:

$$u_e = Q / (\pi (d/2)^2) \tag{3.14}$$

$$u_e = \frac{\Delta P \, d^2}{32 \, \mu L_e} \tag{3.15}$$

From equations (3.8) and (3.10)

$$u = (L/L_e) \; \frac{\varepsilon \, \Delta P (4m)^2}{32 \, \mu L_e} \tag{3.16}$$

$$u = ((L/L_e)^2 \; \varepsilon \; \Delta P \, m^2 \;) / 2 \, \mu \, L \tag{3.17}$$

Substitute m from equation (3.7) in equation (3.17)

$$u = (L/L_e)^2 \frac{1}{k_o} \; \frac{\varepsilon \; \Delta \; P \; \varepsilon^2}{\mu \, L \, S_B{}^2} \tag{3.18}$$

For the most likely pore shapes, circular, rectangular, elliptical and annular, k_o lies in the range of 2.0 to 2.5. The ratio L_e/L is called the tortuosity.

$$u = (L/L_e)^2 \frac{1}{k_o} \; \frac{\varepsilon^3 \; \Delta \; P}{S_V{}^2 (1 - \varepsilon)^2 \, \mu \, L} \tag{3.19}$$

Next we define:

$$k = (L_e / L)^2 \, k_o \tag{3.20}$$

The foregoing are the relationships derived by Kozeny. It has been found experimentally that k = 5.0. In addition $L_e/L = \sqrt{2}$ and k_o =

2.5, which are plausible values for a non-circular cross section.

$$u = \frac{1}{k} \frac{\varepsilon^3}{S_V{}^2(1-\varepsilon)^2} \frac{\Delta P}{\mu L} \tag{3.21}$$

Substitute $u = Q/A$ in equation (3.21)

$$B_o = \frac{Q.L\mu}{A\Delta P} = \frac{1}{5} \frac{\varepsilon^3}{S_V{}^2(1-\varepsilon)^2} \tag{3.22}$$

$$B_o = \frac{1}{5} \frac{F_1}{S_V{}^2} \tag{3.23}$$

Here, A = cross sectional area of bed

F_1 = Kozeny's porosity function = $\varepsilon^3/(1-\varepsilon)^2$

For pure viscous flow, the permeability coefficient B_o is calculated from pressure drop measurement. Then the Kozeny equation gives:

$$B_o = \frac{\varepsilon m^2}{k} = \frac{\varepsilon^3}{k\, S_V{}^2(1-\varepsilon)^2} \tag{3.24}$$

$$= \frac{F_1}{5\, S^2{}_V} \tag{3.25}$$

For gases, it is generally necessary to allow for slip and the calculations are more complex. It is preferable to use a modified permeability coefficient K where:

$$K = \frac{B_o}{\mu} \bar{P} + \frac{4}{3} k_o \bar{v} \tag{3.26}$$

Here, μ = viscosity of air

$\bar{P}$ = average pressure $(P_1+P_2)/2$

$\bar{v}$ = mean thermal molecular velocity

According to the Kozeny equation, modified k_o is defined as:

$$k_o = \frac{\delta}{k'} \varepsilon m \qquad (3.27)$$

Here δ = parameter corresponding to f in flow equation
k' = shape and tortuosity factor for porous media

Substitute m from equation (3.7) in equation (3.27)

$$k_o = \frac{\delta}{k'} \frac{\varepsilon^2}{S_v(1-\varepsilon)} = \frac{\delta}{k'} \frac{F_2}{S_v} \qquad (3.28)$$

Where, F_2 = slip porosity function = $\varepsilon^2 / (1-\varepsilon)$

For a bed of closely- sized spheres of TiO_2, Al_2O_3 and Cr_2O_3 , the value δ / k' or Z is equal to 0.47, which was obtained by Arakawa and Suito (1960).

The symbol $\bar{v}$ is the mean thermal molecular velocity given by:

$$\bar{v} = \sqrt{(8\,RT/\pi M)} \qquad (3.29)$$

Here, R = gas constant [Pa m^3/mole K]
T = absolute temperature [K]
M = air molecular weight [kg/mole]

Substitute B_o , k_o and $\bar{v}$ in equation (3.26)

$$K = \frac{\bar{F}_1 P}{5\,S_v\,2\mu} + \frac{4\,Z\,F_2}{3\,S_v} \sqrt{(8RT/M)} \qquad (3.30)$$

The first term on the right hand side of equation (3.30) expresses the effect of viscous flow and the second term involves the molecular flow.

Contribution of the second term increases either at very low gas pressure or for small pore size since the mean free path of gas molecules becomes comparable to the size of flow space. Hence, when absolute gas pressure is further decreased by keeping the mass flow rate through a porous medium constant, the pressure drop increases because some gas molecules have difficulties penetrating into the smaller pores

or cavities. Since the pore structure, of course, does not change with lowered gas pressure, this phenomenon means that the effective area for gas flow decreases with absolute gas pressure in the molecular flow regime.

Knudsen Number.

The model of gas flow through a porous media mainly is characterized by its viscosity or pressure drop, which is caused by the phenomena of gas molecules colliding with themselves and on solid surface. The number of molecules in a unit volume depends on pressure, temperature and gas species.

Since the experiments of Kundt and Warburg (1875), it has been realized that, if the pressure of a gas flowing in a capillary is reduced until its mean free path is an appreciable fraction of the capillary radius, the rate of flow exceeds that calculated using bulk viscosity in Poiseuille's law or its equivalent. This is attributed to 'slippage' on the capillary walls. If the pressure is further decreased until the mean free path is much greater than the capillary diameter, viscosity plays no part in flow, since molecules collide only with capillary walls, and not with one another. Such 'free molecule' or Knudsen flow is actually a process of molecular diffusion, and takes place for each constituent of a mixture along its own partial pressure, or concentration gradient, even if the total pressure at each end of the capillary is the same.

For ordinary capillaries, slip flow and free-molecular flows occur only at very low pressures. However, in many fine-pored media, their capillary diameters are smaller than or comparable with the mean free path even at atmospheric pressure. It was first realized by Adzumi (1937) that Knudsen number may be used to characterize into four flow regimes as follows:

$Kn < 0.01$	Viscous flow
$0.01 < Kn < 0.1$	Slip flow
$0.1 < Kn < 10$	Transition flow
$10 < Kn$	Knudsen flow or free molecular flow

The present experiments were carried out in the slip and transition flow regimes.

Specific Surface Area of Particles.

A porous refractory is a sintered body made up of an aggregate of particles with different sizes and shapes. Thus the actual flow pattern is very different from that of a simple structure, such as a cylindrical tube. Nevertheless, pressure drop of the medium can be predicted by either a channel model or a drag theory. The former assumes the flow area of the medium as a bundle of channels and pressure drop is related to the specific surface area and porosity of the medium.

According to Arakawa and Suito (1960), pressure drop across a porous medium or a particle packed bed at relatively low absolute pressure is expressed by the following equation:

$$\frac{Q.L}{\Delta P A} = \frac{F_1 \bar{P}}{5(S_v)^2 \mu} + \frac{4Z F_2 \bar{v}}{3 S_v RT} \qquad (3.31)$$

$$\bar{v} = \sqrt{(8RT/\pi M)} \qquad (3.32)$$

$$F_1 = \varepsilon^3/(1-\varepsilon)^2 \qquad (3.33)$$

$$F_2 = \varepsilon^2/(1-\varepsilon) \qquad (3.34)$$

$$Z = 0.47 \qquad (3.35)$$

The first term on the right hand side of equation (3.31) expresses the effect of viscous flow and the second term expresses that of molecular flow and rarefactive effect of slip flow.

At a given mass flow rate, contribution of the second term increases as the gas pressure decreases, so the pressure drop increases. Under this circumstance, the ratio of the mean free path of gas molecules to the pore size becomes large and the rate of collision of gas molecules on the wall surface in close space increases. Since the pore structure, of course, does not change with lowered gas pressure, this phenomenon means that the effective pore area for gas flow decreases with absolute gas pressure in the molecular flow regime.

Consequently, the pore structure of the porous medium can be characterized using the following assumptions:

1. The pore space is distributed isotropically and randomly in the medium, so that surface porosity and volumetric porosity are equal.

2. Pressure drop through the medium is expressible by a channel model, as given by equation (3.31).

From assumption 1, surface and volumetric porosities can be expressed by the following equation using effective mean pore diameters at arbitrary and initial pressures.

$$\varepsilon_V = \varepsilon_S = \varepsilon_{VO} (d/d_O)^2 \qquad (3.36)$$

Since volumetric porosity ε_V, and specific surface area S_V, are given by equations (3.37) and (3.38) using the mean pore diameter d and average pore number in a unit surface area n, S_V can be expressed by equation (3.38).

$$\varepsilon_V = (n \pi d^2)/4 \qquad (3.37)$$

$$S_V = n \pi d \qquad (3.38)$$

$$S_V = 4 \varepsilon_V /d = 4 \varepsilon_{VO} d/d_O^2 \qquad (3.39)$$

Combining equations (3.36) and (3.37) with equation (3.31), the pressure drop becomes a function of a single variable, i.e., either S_V, ε_V or d.

Calculated Pressure Drop per Unit Length.

Kozeny-Carman theory can be expressed in terms of pressure drop per unit length as follows:

For consolidated porous media, Adzumi (1937) modified Kozeny-Carman theory to handle a model of pore space consisting of parallel, uniform, non-circular capillaries, with a length L. Assuming n capillaries of radius r per unit area of cross-section, the porosity, $\varepsilon = n\pi r^2$. The flow equation consists of the free molecular flow region and viscous flow regions and the flow characteristics occur simultaneously under the same pressure drop, as illustrated in figure 3.5.

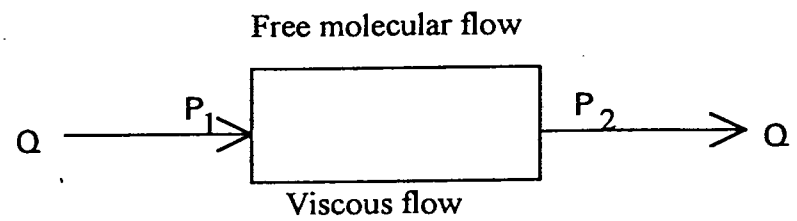

Figure 3.5 Flow Characteristics

Pressure drop in the free molecular flow region as shown in figure 3.6 can be derived as follows:

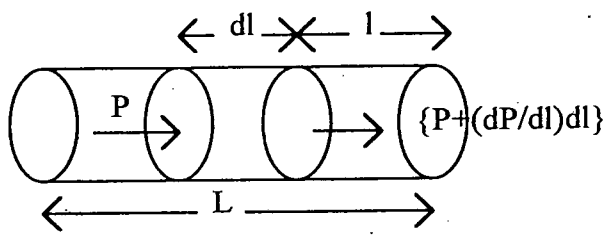

Figure 3.6 Pressure Drop in Free Molecular Flow

$\bar{v}$ is the mean thermal molecular velocity given by:

$$\bar{v} = \sqrt{(8\ KT/\ \pi\ m)} \qquad (3.40)$$

where: K = Boltzmann's constant
m = molecular weight

Root mean square velocity $\sqrt{v^2} = 3KT/m$ (3.41)

The number of molecules hitting on a unit surface area per unit time, ν

$$\nu = (n_o \bar{v})/4 = P / \sqrt{2\ \pi mKT} \qquad (3.42)$$

n_o = molecular concentration
$2\ \pi\ rdL$ = surface area
K = Boltzmann's constant

The total number of molecules hitting on the surface per unit time, N is:

$$N = ((n_o \bar{v})/4)(2\pi rdL) \tag{3.43}$$

The mean gas momentum of one molecules $= m\bar{v}$

Thus the total gas momentum loss on $2\pi rdL$ surface per unit time becomes:

$$R_f = mvN = \frac{-dP.dL}{dL} \tag{3.44}$$

$$\frac{dP}{dL}.dL = -m\bar{v}((n\bar{v})/4)\ 2\pi r\ dL \tag{3.45}$$

$$\frac{dP}{dL}.dL = -mv\ (P/(\sqrt{2\pi mKT}))\ 2\pi r\ dL \tag{3.46}$$

R_f is also expressed as the following equation:

$$R_f = -m\bar{v}P/(\sqrt{2\pi mkT})\ [\bar{v}^2]/[(\bar{v}^2)]\ 2\pi\ r\ dL \tag{3.47}$$

Substituting equation (3.40) and equation (3.41) into equation (3.46)

$$R_f = -m\bar{v}P/(\sqrt{2\pi mKT})\frac{(3KT/m)}{(8KT/m)}\ 2\pi r\ dL \tag{3.48}$$

$$= -(3\pi/8)\ m\bar{v}(P/\sqrt{2\pi mKT})\ 2\pi rdL \tag{3.49}$$

The expression for flow and momentum loss per second is given by:

$$\pi r^2 dP = -(3\pi/8)\ m\bar{v}(P/\sqrt{2\pi mKT})\ 2\pi rdL \tag{3.50}$$

Equation of continuity:

$$\frac{d}{dL}(Pv\,\pi\,r^2) = 0 \qquad (3.51)$$

where: $v\,\pi\,r^2 =$ volume/second

Integrating equation (3.51), we have:

$$Q_o = (Pv\,\pi\,r^2)dL = -(4/3)\,r^3\,\sqrt{2\,\pi\,KT/m}\;dP \qquad (3.52)$$

$$(PV)_T\,L\,\Big|_o^L = -\frac{4}{3}\,r^3\,\sqrt{(2\,\pi\,KT)/m}\;P\,\Big|_{P_1}^{P_2} \qquad (3.53)$$

$$(PV)_T = \frac{4}{3}\,\frac{r^3}{L}\,\sqrt{2\,\pi\,KT/m}\;(P_1-P_2) \qquad (3.54)$$

$$Q_o = q(\text{mole/sec}) = \frac{(PV)_T}{RT} = \frac{4}{3}\,\frac{r^3}{L}\sqrt{2\,\pi/(mKT)}(P_1-P_2) \qquad (3.55)$$

For pressure drop in the viscous flow region through a permeable refractory pore, the Hagen-Poiseuille equation holds:

$$Q = \frac{r^4\,\Delta P}{8\,\mu\,L} \qquad (3.56)$$

where: $Q_o =$ mole/sec

$$Q = MQ_o/\rho = (RT/P)Q_o \qquad (3.57)$$

Equation (3.55) becomes:

$$Q_o = (1/RT)\,\frac{\pi\,r^4\bar{P}\,\Delta P}{8\,\mu\,L} \qquad (3.58)$$

The flow equation is obtained by adding the Kozeny-Carman equation and the viscous flow equation:

$$Q = \text{Viscous flow} + \text{Free molecular flow}$$

$$Q = \frac{1}{RT\,L}\,\Delta P\left(\frac{\pi P}{8\mu} r^4\right) + \frac{4}{3} r^3 \sqrt{\pi RT/2M}\;E) \qquad (3.59)$$

$$E = \text{empirical factor}$$

$$E = \frac{1 + (2/\mu)\sqrt{M/RT}\; r\,\bar{P}}{1 + (2.47)/\mu)\sqrt{M/RT}\; r\,\bar{P}} \qquad (3.60)$$

$$\bar{P} = (P_1 + P_2)/2$$

Mean Free Path.

The mean free path λ of a molecule is the average distance traveled by a molecule before collision with another and may be expressed by the following equation:

$$\lambda = \frac{KT}{\sqrt{2}\,\pi\,(2r)^2 P} \qquad (3.61)$$

$$\lambda = \frac{1}{\sqrt{2}\,\pi\,(2r)^2 n} \qquad (3.62)$$

n = molecular density

$$n = \frac{P}{KT} \Rightarrow P = nKT \qquad (3.63)$$

K = Boltzmann's constant = 1.380257×10^{-23} J/molecule K

$$r = r_\alpha (1 + T_V/T) \qquad (3.64)$$

T_V = 293.15 K for 20 °C

T = room temperature

r_α = molecular radius (for $T = \alpha$)

For N_2 : r = 1.85×10^{-8} cm.

r_α = 1.60×10^{-8} cm.

For O_2 : r = 1.8×10^{-8} cm.

r_α = 1.48×10^{8} cm.

Molar ratio of N_2 : O_2 in air = 3.762:1 or 79:21

$[N_2]$: $[O_2]$

r for $N_2 = 3.762 \times 1.85 \times^{-8}$: r for $O_2 = 1 \times 1.8 \times 10^{-8}$

r for $N_2 = 6.9597 \times 10^{-8}$: r for $O_2 = 1.8 \times 10^{-8}$

$$r_{air} = \frac{(6.9597+1.8)X10^{-8}}{(3.762+1)} = 1.8395 \times 10^{-8} \text{ cm}$$

$$= 1.8395 \times 10^{-10} \text{ m}$$

r_α for $N_2 = 3.762 \times 1.6 \times 10^{-8}$: r_α for $O_2 = 1 \times 1.48 \times 10^{-8}$

r_α for $N_2 = 6.0192 \times 10^{-8}$: r_α for $O_2 = 1.48 \times 10^{-8}$

$$r_\alpha \text{ for air} = \frac{(6.0192+1.48) \times 10^{-8}}{(3.762+1)} = 1.5748 \times 10^{-8} \text{ cm}$$

$$\lambda = \frac{1}{\sqrt{2}\ \pi\ (2 \times 1.8395 \times 10^{-10})^2} \frac{KT}{P} \qquad (3.65)$$

$$= \frac{1}{\sqrt{2}\ \pi} \frac{\times 1.380257 \times 10^{-23}}{(3.679 \times 10^{-10})^2} \frac{T}{P}$$

$$= \frac{1.380257 \times 10^{-23}}{60.134603 \times 10^{-20}} \frac{T}{P}$$

$$= \frac{2.295279 \times 10^{-5}}{P} T \qquad (3.66)$$

$= 6.64 \times 10^{-8}$ m for air at T =293.15 K, and P=1.013×10^5 Pa

The mean free path of gas molecules λ is a function of absolute pressure and absolute temperature which are known. Consequently, the pore structure can be characterized by plotting S_V, or ε_V, against λ.

Pore Diameter and Permeability.

Effect of particle diameter according to Poiseuille's law, if a capillary has a diameter d_e, the rate of flow through it under a given pressure gradient is proportional to d_e^2. Thus, if the pore space is taken as equivalent to a bundle of capillaries of uniform diameter d_e and Dupuit's relation is applied, we have:

$$u \ \alpha \ \varepsilon \, d_e^2 \qquad (3.67)$$

Various attempts have been made to derive the correct relationship of the mean pore diameter, d_e, to other quantities. The simplest packed bed is one of uniform spheres, and it is not unreasonable to assume that all such beds with random packing and of equal porosity are geometrically similar. It would then follow that the mean pore size is proportional to particle diameter d, and therefore:

$$u \ \alpha \ \bar{d}^2 \qquad (3.68)$$

The relation between permeability (K), apparent porosity (P_o) and mean pore diameter (d_e) can be expressed by equation (3.69):

$$K = k_o \ P_o \, (\bar{d})^2 \qquad (3.69)$$

where: $k_o = 1/80 \ \mu$ (μ is viscosity of air)

That is, this equation indicated that K is linear when plotted against $P_o \, (\bar{d})^2$ using a log scale.

Fractal Geometry.

1. General Background.

The word "fractal" was coined by Benoit Mandelbrot in the mid 1970. Actually, this subject has a long and interesting history in mathematics, involving many mathematicians from many parts of the world over the past centuries, including Peano from Italy, Cantor and Hausdorff from Germany, Besicovith from Russia, and many others. Mandelbrot realized that the bizarre, seemingly contrived geometric constructions engineered by these mathematicians were not at all

pathological, as they were at first regarded. Rather, he showed that many everyday objects such as coast lines, snowflakes, clouds, leaves, ferns and mountain ranges were naturally described by fractals. Ordinary geometry constructions using straight lines, smooth curves and surfaces did not help very much to understand or to model many intricate patterns found in nature. Thus was born a new branch of mathematics, called fractal geometry. This field of mathematics has proved to be extremely useful in a variety of applications. Even Hollywood has made use of fractal geometry to create fractal landscapes and planet- scapes for films.

Mandelbrot (1982) originally offered the following tentative definition of a fractal:

" A fractal is by definition a set for which the Hausdorff-Besicovitch dimension strictly exceeds the topological dimension"

This definition requires further definition of the terms "set", "Hausdorff-Besicovitch dimension (D)" and "topological dimension (D_T)", which is always an integer. A fractal may be considered to be sets of points embedded in space. For example, the set of points that make up a line inordinary Euclidean space has the topological dimension $D_T = 1$, and the Hausdorff-Besicovitch dimension $D = 1$. Since $D = D^T$ for the line, it is not fractal according to Mandelbrot's definition, which is reassuring. Again, Mandelbrot suggests that such curves as stated in figure (3.7) can have their ruggedness described by allocating a fractional number between one and two that will describe their space-filling ability. The difference between topological dimension and Euclidean dimension indicates the existence of fractal dimension.

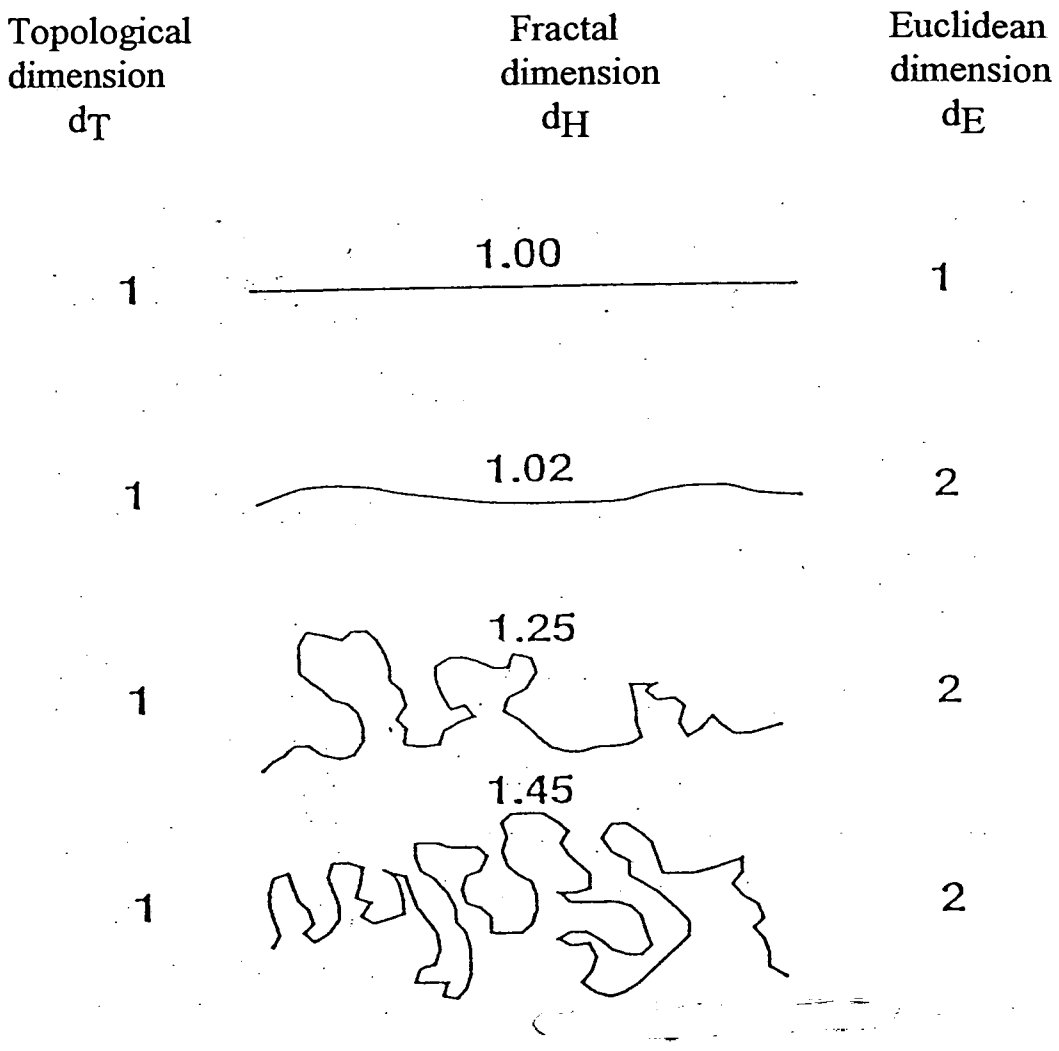

Figure 3.7 Topological, Fractal, and Euclidean Dimensions of Rugged Lines

In fact Mandelbrot (1986) has retracted the above tentative definition and proposes instead the following:

"A fractal is a shape made of parts similar to the whole in some way" Basically, a fractal is a geometric shape that has two special properties:

1. The object is self-similar
2. The object has fractional dimension

An object normally considered as one-dimensional, for example, a line segment, also possesses a self-similar scaling property. A line can be divided into N identical parts, each of which is scaled down by

the ratio $r = 1/N$ from the whole. Similarly, a two-dimensional object, such as a square area on a plane, can be divided in N self-similar parts, each of which is scaled down by a factor $r = 1/\sqrt{N}$ or $1/N^{1/2}$. A three-dimensional object like a solid cube may be divided in N little cubes, each of which is scaled down by a ratio $r = 1/(\sqrt[3]{N}) = 1/(N)^{1/3}$. With self-similarity the generalization to fractal dimension is straight forward. A D-dimensional self-similar object can be divided in N smaller copies of itself, each of which is scaled down by a factor r where $r = 1/(\sqrt[D]{N})$ or $N = 1/(r^D)$. Conversely, given a self-similar object of N parts scaled by a ratio r from the whole, as given in table 3.3, its fractal or similarity dimension is given by:

$$D = \frac{\log(N)}{\log(1/r)} = -\frac{\log(N)}{\log(r)} \qquad (3.70)$$

Table 3.3 Scaling Law for Fractional Dimension

Object	Number of pieces	Scaling	Law
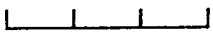	3	1/3	$3 = 3^1$
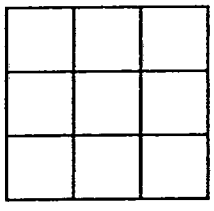	9	$1/(3^{1/2})$	$9 = 3^2$
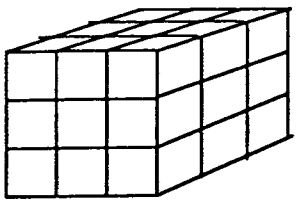	27	$1/(3^{1/3})$	$27 = 3^3$

2. Fractal Analysis of Pore Shape.

Fractal analysis is another method to evaluate the random structure. A fractal is defined as an extremely irregular line (or surface) formed of an infinite number of similarly irregular sections (or parts). A fractal has fractional dimension between one and two (or between two and three). The extremely irregular pore shape, as represented by the periphery of the pore cross section, may be treated as a fractal.

Let N(r) be the counted number of subsections (squares of side r) containing at least one small part of any pore when the representative length of each subsection is r, the so-called similarity ratio.

For a fractal, the following equation holds:

$$N(r) = (\text{Similarity ratio})^{-D} = r^{-D} \qquad (3.71)$$

Here the fractal dimension, D is defined by:

$$D = -\frac{\log N(r)}{\log (r)} \qquad (3.72)$$

All cut specimens were micro-photographed using a reflecting microscope. An example of the counting N(r) was shown in figure 3.8. In short, the similarity ratios r were halved consecutively from 1/2, 1/4, 1/8, to 1/128 and the count N(r) was counted as a function of r.

The relationship between N(r) and r was plotted on log-log scales as shown in the figure, and the fractal dimension was calculated from the slope of the convergent straight lines in figure 3.9.

I 1719605 X

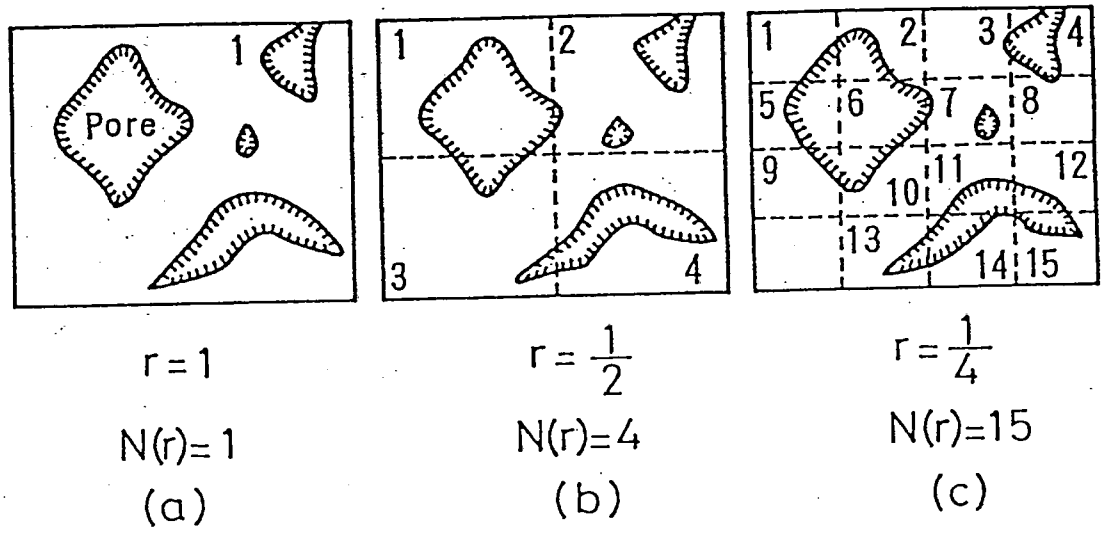

Figure 3.8 Measurement of Fractal Dimension

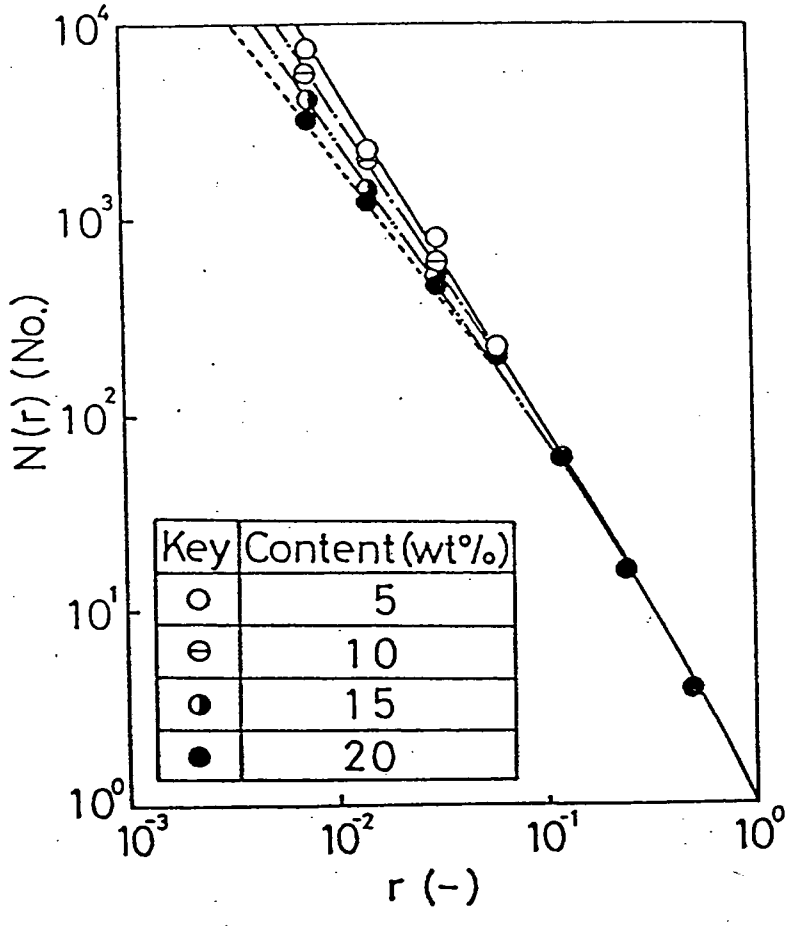

Figure 3.9 Sample of Fractal Dimension Plotting

Image Analysis.

1. Overview and History.

Image analysis has become an accepted method of morphological quantification in a wide variety of research fields. The first image analysis systems appeared in the 1960's in the form of analog video signal processors, that were capable of making basic measurements of relative areas by selecting and discriminating voltage thresholds of the video signal. These systems were not able to measure individual morphologies or to calibrate gray levels.

The advent of small powerful computers in the late 1970's and early 1980's brought about a whole new generation of image analysis systems based on the early personal computers attached with dedicated processor elements. The video signals were then digitized and stored in a memory array. By having this permanent digital representation of an image in the memory, one was able to perform far more complex measurements, such as calculating morphology of individual objects and calibrating density transformations from the representative voltages in the original video signal.

Today's systems have evolved from the abundance of inexpensive mass memory and faster, higher resolution data processing integrated circuits. Based mainly on IBM-PC technologies, typical systems allow users not much familiar with computer technology to make automated program sequences (commonly called MACROS) by just pointing at a sequence of instructions on a menu, resulting in the extraction of morphological and densitiometric data. These data may be further evaluated to provide graphical and statistical evaluations, all within a single software package.

2. Basic Concepts of Image Analysis Processing.

The main components of any modern image analysis system are a video camera, analog to digital conversion circuitry to convert the analog video signal to digital, computer system with dedicated image memory separate from the system program memory, display monitors for program control and image display, and peripheral devices to provide hard copy of the derived data and/or image printout. The software should be

flexible enough that applications can be adapted to a wide variety of user's needs, rather than limited to single dedicated usage. This means that user-defined sequences along with pre-defined application examples may be modified when and if necessary. It is also important that the hardware components are of an open architecture allowing future upgrading of dedicated or off-the-shelf components.

Once an image is digitized, it is stored as an array of picture elements, or pixels, with a gray value resolution comparable to the input camera or scanning device (SEM, TEM, STM, AFM, etc.). Once in this form the image can be treated as data arrays and mathematical algorithms applied. These algorithms act to enhance certain features within the image (such as edge detection , delineation , contour enhancement) and can be likened to the various contrast enhancement techniques and filtering methods used in optical microscopy. Once the features of interest have been extracted, the gray level image is segmented into a binary image (dissected to black and white essentially). Further feature extraction may now be performed through, for example, erosions, deletions, skeletonizations and the extracted image can be overlaid easily on the original image for comparisons.

At this point, the binary image can be identified for each individual object and coded with an arbitrary color and measured. The measurements fall into three categories, object specific (where information related to each object is measured), field specific (where percentages of the total image area are extracted), and densitiometric (where the image gray values are transformed to calibrated density or reflectance values with respect to objects or the total field). Measured values can be combined to provide additional information such as estimated volumes and surface areas. These data are typically stored on diskette for further statistical evaluations.

The more comprehensive image analysis systems today allow for easy data format translation to external computer programs and usually include a comprehensive set of statistical and data classification functions with complete graphic display of the measured values.

3. Color Images.

Certain image preparations include colored stains or color polarization microscopy effects, with different hues of color. The images can be treated in the same way, except that the input is taken as 3

separate image slices corresponding to the red, green and blue components. These are then treated in the same way and can be discriminated based on the color hue and densities.

Another method of color analysis is to apply pseudo (or false) color to monochrome images. This technique requires that a color table corresponding to the gray levels in the image is created and then the color are displayed over the image. Rather than making actual measurements of the features, the colors can now be visually evaluated since the human eye perceives differences in color much better than slight variations of gray tones.

4. Benefits of Image Analysis.

It is clear that image analysis techniques allow for the easy acquisition of large sets of sample data, leading to better statistical accuracy. One other great benefit is that human subjectivity is almost completely removed. Once a standard MACRO is defined, each subsequent measurement is completely independent of the user and results are easily correlated. With the advent of larger; cheaper data mass storage devices, images can be kept as a permanent record in the original resolution and recalled at a later date for further evaluations. This is a key benefit over the storage of preparations that degrade over time. It is also difficult, if not impossible, to reproduce critical preparation at a later date.

The image analysis is an important technique for directly characterizing the particle geometry or porous structure geometry.

Table 3.4 Basic Image Processing and Analysis Steps

Image Input ↓	* Grabbing and digitization of video or slow-scan image data to delicate memory * Importing disk file image * Digitizing video tape images
↓ Calibration	* Scaling of pixels (picture elements) to "Real Life" units e.g., UM, MM, KW * Scaling of gray levels to density units, e.g.,

optical density, transmission, reflection and enhancement

↓

Enhancement

* Extraction and enhancement of features of interest via digital filter, e.g. contours, feature boundaries, textures

↓

Segmentation

* Separation of features of interest into a binary image masking out other artifacts in the image

↓

Measurement

* Individual object morphologies
* Individual object densities
* Field areas (percentage of total image area)

↓

Data Output

* Disk storage of individual or accumulated data
* Hard copy printout of individual or accumulated data
* Graphic representations
* Statistical evaluations

5. Advantages of Image Analysis.

* Completely objective results
  i.e. human subjectivity is completely removed providing higher accuracy of measurements

* Increased measurement speed as compared to scale grid comparisons and point count measurements

* Higher sample throughput via sequence automation

* Partially automated diagnosis capability through program automation

* Permanent digital record of original preparation for future

analysis

6. Field Specific Measurements.

e.g. Image Size = 640 x 512 pixels

Total Field Area
= 640 x 512 Pixel
= 327,680 Pixels^2
= 100%

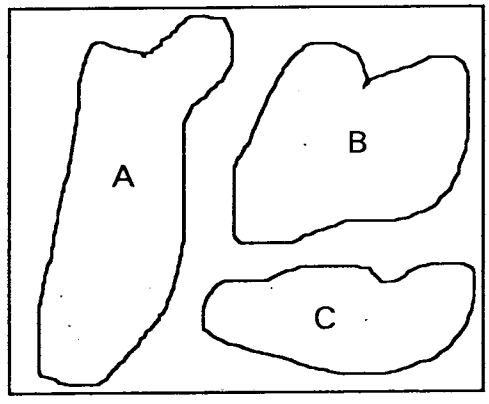

Figure 3.10 Field Specific Measurement

$$\text{Relative Area \% (Area Percent)} = \frac{(\text{Area A} + \text{Area B} + \text{Area C})}{\text{Total Area}} \times 100$$

Field Perimeter	=	Perim A + Perim B + Perim C
Intercepts	=	# of Horizontal Intercepts in the Image
Sum of Chord Lengths	=	Chords A + Chords B + Chords C
Reference Chord Length	=	(64O Pixels x 512 Lines) = 327,680 Chords
Total Image Area	=	(Area A + Area B + Area C)

Solid solution.

Solid solution (s.s) occurs when chemical compounds react during sintering. The following are typical solid solution reactions:

$$Al_2O_3 + TiO_2 \xrightarrow{1,573K} Al_2O_3.TiO_2 \quad (3.73)$$

$$MgO + Al_2O_3 \xrightarrow{1,273\text{-}1,373K} MgO.Al_2O_3 \quad (3.74)$$

$$MgO + 2TiO_2 \xrightarrow{1,273K} MgO.2TiO_2 \quad (3.75)$$

$$2MgO + TiO_2 \xrightarrow{1,373K} 2MgO.TiO_2 \quad (3.76)$$

$$[MgO.Al_2O_3] + TiO_2 + Al_2O_3 \rightarrow \begin{cases} TiO_2.Al_2O_3 & (3.77) \\ (TiO_2.Al_2O_3)\text{-}MgO.2TiO_2 \text{ s.s} & (3.78) \\ (MgO.Al_2O_3)\text{-}2MgO.TiO_2 \text{ s.s} & (3.79) \end{cases}$$

In equation (3.75), when TiO_2 is added, product of $MgO.2TiO_2$ increases. Similarly equation (3.78) $TiO_2.Al_2O_3$-$MgO.2TiO_2$ s.s also increases when TiO_2 and Al_2O_3 react with $MgO.Al_2O_3$.

In the glossy area, $Al_2O_3.TiO_2$, $MgO.Al_2O_3$-$2MgO.TiO_2$ s.s and $TiO_2.Al_2O_3$ -$MgO.2TiO_2$ s.s coexist with each other. Figure 3.11 showed the system reaction.

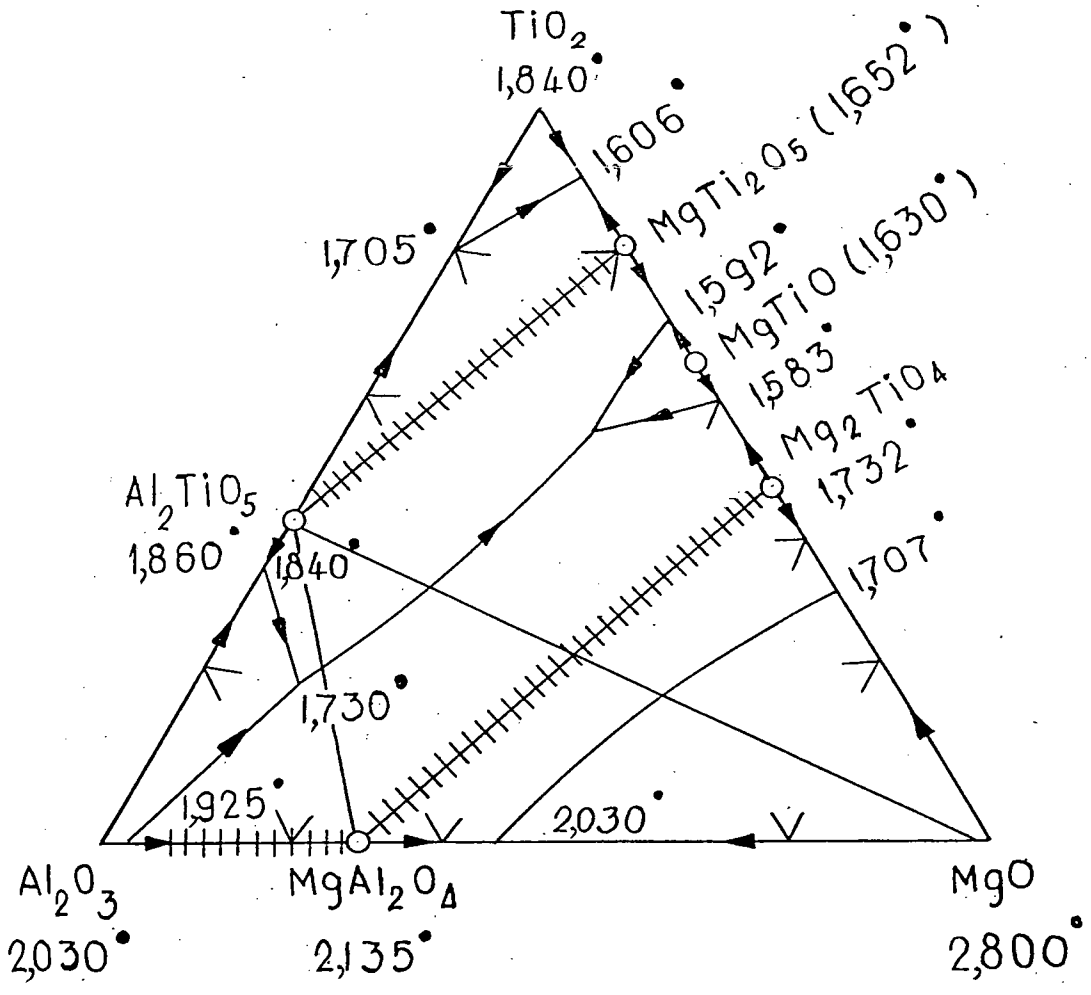

Figure 3.11 System $MgO-Al_2O_3-TiO_2$, Primary Phases (Cross Hatched Lines Are Solid Solutions)